Modeling the collapse of the edge when two transition routes compete

Miguel Beneitez [1,*] Yohann Duguet [2,†] and Dan S. Henningson [1,‡]

[1]*Linné FLOW Centre and Swedish e-Science Research Centre (SeRC), KTH Engineering Mechanics,*
Royal Institute of Technology, SE-10044 Stockholm, Sweden
[2]*LIMSI-CNRS, Université Paris-Saclay, P91405 Orsay, France*

The transition to turbulence in many shear flows proceeds along two competing routes, one linked with finite-amplitude disturbances and the other one originating from a linear instability, as in, e.g., boundary layer flows. The dynamical systems concept of an edge manifold has been suggested in the subcritical case to explain the partition of the state space of the system. This investigation is devoted to the evolution of the edge manifold when linear stability is added in such subcritical systems, a situation poorly studied despite its prevalence in realistic fluid flows. In particular, the fate of the edge state as a mediator of transition is unclear. A deterministic three-dimensional model is suggested, parametrized by the linear instability growth rate. The edge manifold evolves topologically, via a global saddle-loop bifurcation of the underlying invariant sets, from the separatrix between two attraction basins to the mediator between two transition routes. For larger instability rates, the stable manifold of the saddle point increases in codimension from 1 to 2 after an additional local pitchfork node bifurcation, causing the collapse of the edge manifold. As the growth rate is increased, three different regimes of this model are identified, each one associated with a flow case from the recent hydrodynamic literature. A simple nonautonomous generalization of the model is also suggested in order to capture the complexity of spatially developing flows.

I. INTRODUCTION

After more than a century of theoretical, experimental, and computational progress, predicting the transition from laminar to turbulence in usual fluid flows is still a puzzle for mathematicians, physicists, and engineers [1,2]. The situation appears even more complex when different routes toward the same turbulent state are in competition. The theory of dynamical systems is an elegant way to rationalize such situations because it provides a cartography of the space of possible initial conditions depending on their outcome at a later time. The key concepts here are those of basins of attraction and boundaries separating disjoint basins of attraction [3]. For purely supercritical systems such as corotating Taylor-Couette flow or the Rayleigh-Bénard setup, transition to a nontrivial state is triggered by any infinitesimal disturbance provided the control parameter (usually the Reynolds number or the Rayleigh number) exceeds a given threshold [4]. In such a case, the whole state space becomes the attraction basin of

this nontrivial state. After several bifurcations as the control parameter is increased, the nontrivial state can be identified with turbulence. For classical subcritical systems such as pipe or plane Couette flow, the state space is usually partitioned into two basins of attraction, one for the laminar state and the other one for the turbulent one [2,5] for the appropriate Reynolds number. When both the laminar and the turbulent regime are attracting sets (in the sense that trajectories stay in their neighborhood for arbitrary large times), the basin boundary common to these two basins is a smooth hypersurface called *the edge* [6]. The edge is an invariant set for the flow dynamics, and it is of codimension 1. In the simplest case, it is the stable manifold of a given unstable state called *the edge state*, a relative attractor within that manifold [7]. The most popular method to identify the edge state(s) of the system relies on bisection [5,8]. Alternatives to this approach have been suggested but usually rely on some preknowledge of the dynamical nature of the edge state [9–11]. The study of the edge manifold becomes mathematically more complex in a situation relevant for the lowest Reynolds numbers close to the onset of transition: the turbulent set, although still a chaotic set, is no longer an attractor. Trajectories visiting it have a finite probability to reach the laminar state after an arbitrarily long transient time [6,12,13]. This has led to a generalization of the concept of an edge manifold, seen as a boundary between two types of trajectories that happen to have the same asymptotic outcome, namely the laminar regime. Reference [14] introduced a distinction, depending on whether the edge manifold splits the state space into two disjoint attractions basins (hard type) or not (soft type).

*beneitez@kth.se
†duguet@limsi.fr
‡henning@kth.se

Conceptually, there is a symmetric configuration that has been little studied so far despite its relevance to transitional flows at high Reynolds numbers: what happens to the edge manifold in the case in which the laminar state loses its laminar stability (while the turbulent state remains attracting)? Such a linear instability of the laminar state in an otherwise subcritical fluid system occurs at least in three of the most important examples of shear flow transition: the flow inside a curved pipe [17], inside a parallel channel [18], and the Blasius boundary layer flow developing over a flat plate [19]. In these cases, the subcritical nature of the transition (the bypass transition scenario) is in competition with the exponential growth, followed by their destabilization, of the so-called Tollmien-Schlichting (TS) waves (the classical transition scenario) [20]. Even in the absence of such well understood linear instability, other general destabilization mechanisms can be in competition with the usual bypass picture: the presence of small roughness at the walls [21], geometrical defect to the base flow [22], or, among other possibilities, competing instability mechanisms due to additional parameters [23]. Several important fundamental questions arise in such cases: what happens to the basin boundary and to its role as a mediator of transition [24]? Can edge states still be identified, and what is their role in the state space? Does the geometric notion of an edge manifold at least make sense mathematically speaking? Is there any way to select or control a given transition route at the expense of the other one? Can low-order models faithfully reproduce the complex dynamics at play, and if so, to what extent?

The three canonical cases of curved pipe flow, plane channel flow, and the Blasius boundary layer have been assessed numerically in very recent investigations. For curved pipe flow, finite curvature leads, above some threshold in the Reynolds number, to an additional instability absent from the straight pipe case [25]. This instability leads to a limit cycle replacing the laminar state. The edge manifold generalizes hence to the separatrix between the turbulent state and a new attractor replacing dynamically the traditional laminar fixed point. In plane Poiseuille flow, for the parameters chosen in the corresponding study, the edge state is a traveling wave solution appearing in a saddle-node bifurcation at a finite Reynolds number $R \approx 459$, while the instability of the base flow to TS waves does not occur before $R = 5815$ [26]. As R is increased from low to high values, the classical route emerges in parallel to the bypass route, and it concerns an increasingly large subset of the state space of initial conditions [26]. However, for $R = 5855$ it is reported that the edge state still exists as a finite-amplitude traveling wave, whose stable manifold still separates the initial conditions leading to the turbulent state by involving TS waves from those who lead to a transition without TS waves taking an active role. The case of the Blasius boundary layer, despite its relevance to transition in wind tunnels, presents additional difficulties for bifurcation studies: because of the spatial development of the laminar base flow in the downstream direction, there is no independent control parameter. A Reynolds number can be constructed as in most flows, however it should be interpreted instead as a spatial coordinate [19]. There, the bisection algorithm has also been employed in order to determine an edge trajectory converging neither to the laminar nor to the turbulent state.

The computational cost of the whole approach, linked to the cost of simulating a spatially extended three-dimensional flow field, made conclusions ambiguous until recently. The bisection method successfully identifies a recognizable spatially localized coherent structure over moderate finite times in the form of a long velocity streak [16,27]. However, for even larger horizon time it becomes increasingly ambiguous to label a given trajectory as transitioning via the bypass or classical route [15]. This results in a failure of the standard bisection algorithm for the asymptotic edge regime. An illustration of the two different routes to turbulence starting from nearby initial conditions is shown in Fig. 1 using a physical space visualization [28] and state portraits. The state space visualizations in Figs. 1(a) and 1(b) show that despite a common initial path, the two trajectories separate rapidly but converge later toward the same turbulent regime. The physical space visualizations in Figs. 1(c) and 1(d) highlight the very different coherent structures present along either route: elongated in the streamwise direction for the bypass route, in the spanwise direction for the classical route. The three present examples, based on realistic Navier-Stokes simulations, correspond to three scenarios distinct from the classical bistable picture presented in [5]. This wealth of behaviors suggests that a better understanding of the fate of the edge manifold is welcome as soon as a linear instability competes with an already existing subcritical transition picture. Low-dimensional models of subcritical transition have proven a strong companion tool for an improved understanding of dynamical features such as the role of the edge in transition [29–34]. In this tradition, we suggest here a nonlinear model of subcritical transition, inspired by the two-dimensional model in Ref. [29] to which a linear instability mechanism is added consistently with all the hydrodynamic constraints. As we shall see, the suggested autonomous model parametrized by the unstable growth rate displays three parameter regions of interest. In region I, several local bifurcations change the attracting laminar state without altering the global structure of the state space, a dynamical regime qualitatively akin to Ref. [25]. In region II, the state space structure is globally modified after a global bifurcation, and only one basin of attraction remains while the edge state still exists, similarly to Ref. [26]. In region III, the edge state ceases to exist and the edge collapses, qualitatively closer to the dynamics reported in Ref. [15]. The study of these regions, together with an extension to a nonautonomous system, allows for an explanation of all the dynamical regimes displayed by the previous fluid flow examples and suggests new directions.

The issues raised in this article go easily beyond the realm of hydrodynamic transition to turbulence. Any nonlinear dissipative system with two competing attracting regimes is concerned with the notion of basin boundary and edge manifold. At the level of modeling, many of the low-order models from mechanics show strong similarities with the models used in hydrodynamics [11,35–37]. The generalization of the edge concept suggested using the present model is hence of interest for many dissipative bistable systems.

The paper is structured as follows: the reference two-dimensional Dauchot-Manneville system is introduced together with its autonomous three-dimensional generalization in Secs. II A and II B, respectively. The parametric analysis
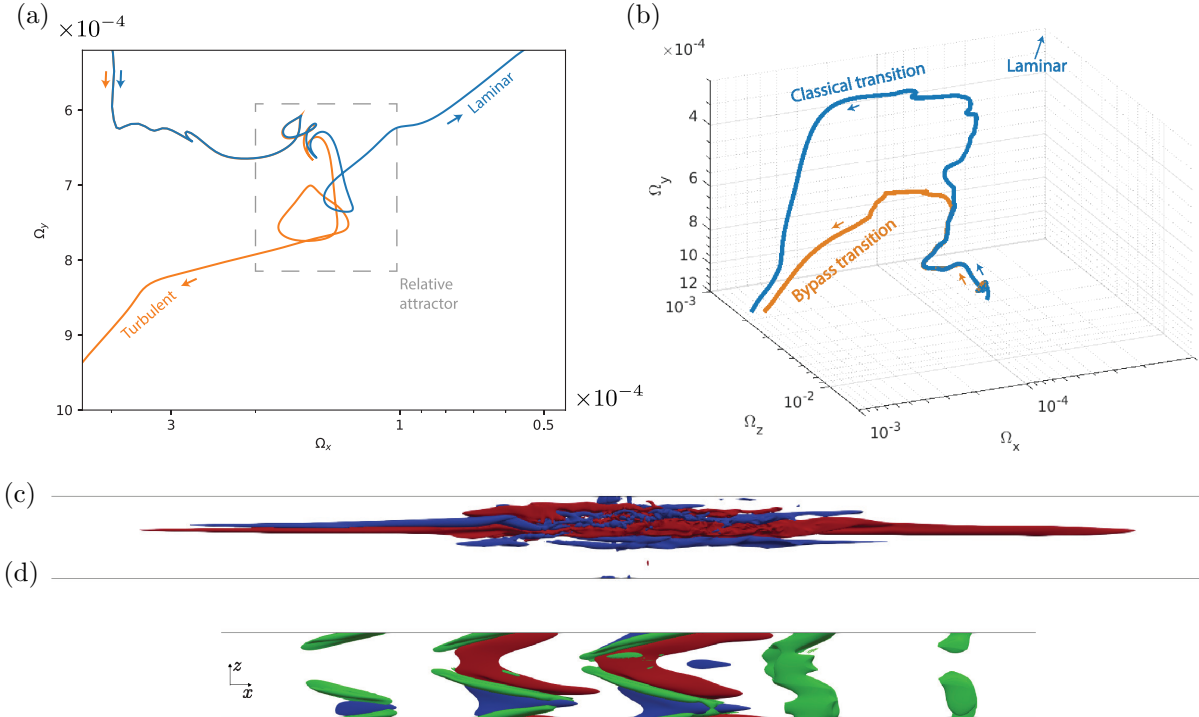
FIG. 1. Edge tracking in Blasius boundary layer (see [15] for a detailed study). (a) State portrait at moderate times $t \approx [0, 5000]$ using the vorticity variables Ω_x and Ω_y defined in [15,16]. (b) State portrait at large times $t \approx [700, 14\,000]$ using the variables Ω_x, Ω_y, and Ω_z. Trajectories correspond to the classical transition route approaching the laminar state (blue) and the bypass transition route (orange). (c),(d) xz-view of three-dimensional perspective along two different coexisting transition routes. Contours of $\lambda_2 = -9 \times 10^{-6}$ (green), isosurfaces of streamwise perturbation velocity with respect to the spanwise mean with values $= 0.06$ and -0.08 (red and blue, respectively), flow from left to right. (c) Bypass transition. (d) Classical transition.

of the 3D model is carried out in Secs. II C, II D, and II E. A nonautonomous version of the model is introduced and analyzed in Sec. III. Eventually, the relevance of the two models to the original hydrodynamical context is discussed in Sec. IV.

II. LOW-ORDER MODELS OF SHEAR FLOW

We consider shear flow models in the spirit of the Galerkin models derived from the Navier-Stokes equations (see, e.g., [11] for a recent review). Galerkin models are obtained by projecting the original partial differential equations onto a basis of predetermined spatial functions called "modes." The use of divergence-free modes is such that the pressure terms have zero projection on the resulting subspace. The generic structure of such models is hence a simple ordinary differential equation in time of the form

$$\dot{\boldsymbol{x}} = \boldsymbol{f}(\boldsymbol{x}) = \boldsymbol{L}\boldsymbol{x} + \boldsymbol{N}(\boldsymbol{x}), \tag{1}$$

where $\boldsymbol{x} \in \mathbb{R}^n$, n being a small integer, contains the relevant degrees of freedom of the system. $\boldsymbol{L}$ is the linear operator corresponding to the system linearized around the origin $\boldsymbol{x} = \boldsymbol{0}$, and $\boldsymbol{N}(\boldsymbol{x})$ represents the nonlinear terms. The model is such that the origin $\boldsymbol{x} = \boldsymbol{0}$ corresponds to the laminar fixed point L, while the turbulent state is simply represented by a different (attracting) fixed point T.

As pointed out in Ref. [30], for a model of subcritical transition to be consistent with the original PDEs it needs to be

subjected to two constraints: (i) $\boldsymbol{L}$ is a linearly stable operator (i.e., all its eigenvalues have real negative parts), which allows for non-normal growth; (ii) $\boldsymbol{N}(\boldsymbol{x})$ conserves the total energy of the system, i.e., $\langle \boldsymbol{N}(\boldsymbol{x}), \boldsymbol{x} \rangle = 0$ for all $\boldsymbol{x}$, where $\langle \cdot, \cdot \rangle$ is the scalar product. The constraint (i) is a property of the linearized Navier-Stokes operator that characterizes the subcritical flow cases of interest [38]. The constraint (ii) is an implication from the Reynolds-Orr theorem $\int (\boldsymbol{v}\nabla\boldsymbol{v}) \cdot \boldsymbol{v} d^3\boldsymbol{x} = \boldsymbol{0}$, itself derived directly from the Navier-Stokes equations for periodic or localized flow fields [19].

The numerical solutions of the ODEs presented in this work have been obtained using Julia [39] with the package DifferentialEquations.jl [40]. The solver used is `Tsit5()` with relative and absolute tolerances of 10^{-14}.

A. Dauchot-Manneville model

One of the simplest Galerkin models of shear flows was introduced by Dauchot and Manneville in Ref. [29]. The model (hereafter referred to as DM2D) is autonomous and assumes a two-dimensional state space. In its original form, the components of $\boldsymbol{x} = (x_1, x_2)$ are meant as the amplitudes of specific Fourier modes with wave numbers k and $2k$ in a physical direction z, in the spirit of Galerkin's projections. The associated velocity field in physical space reads $v = x_1 \sin z + x_2 \sin 2kz$. Its self-interaction via the nonlinear terms $v\partial_z v$ from the Navier-Stokes equations has no contribution on the equation for x_1, and induces the inertia term $-kx_1^2$ when projected on
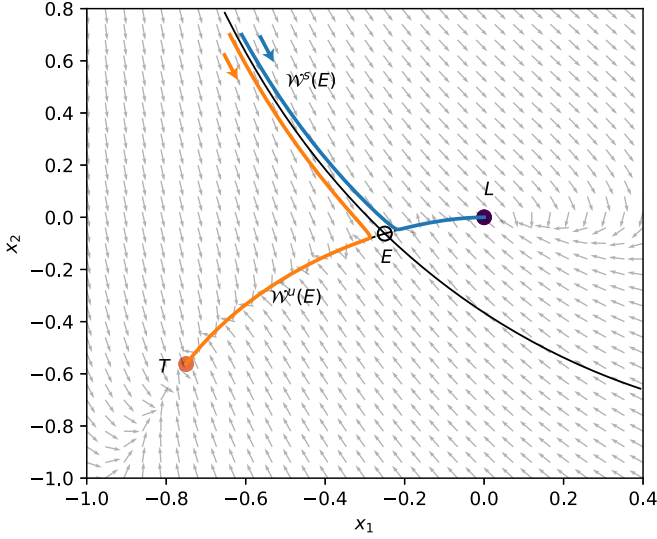
FIG. 2. Phase portrait of the 2D Dauchot and Manneville model. It is also the state portrait of the 3D model (independently of the value of s_3) restricted to the invariant plane $\mathcal{P}$ defined by $x_3 = 0$. Two trajectories approaching T and L are shown in orange and blue, respectively.

the equation for x_2. This suggests to consider in the model a quadratic nonlinearity N satisfying both this property as well as the constraint $\langle N(x), x \rangle = 0$ previously mentioned. The simplest such form for N is $(N_1, N_2) = (x_1 x_2, -x_1^2)$. The linear operator L is directly inspired from Trefethen's model [38].

The equations for the DM2D model read

$$\frac{dx_1}{dt} = s_1 x_1 + x_2 + x_1 x_2, \tag{2}$$

$$\frac{dx_2}{dt} = s_2 x_2 - x_1^2, \tag{3}$$

where $s_1 < 0$ and $s_2 < 0$ are two real parameters interpretable as decay rates. The corresponding operator L is non-normal and definite negative. The effective control parameter in this two-dimensional model is the discriminant $\Delta = 1 - 4 s_1 s_2$. We restrain the analysis to the range $\Delta < 1$. For $\Delta < 0$ there is only one fixed point $L = (0, 0)$. Two additional fixed points called E and T appear in a saddle-node bifurcation at $\Delta = 0$. They are, respectively, unstable and stable, and their expressions are

$$E = \left(\frac{1}{2}(-1 + \sqrt{\Delta}), \frac{1}{4 s_2}(-1 + \sqrt{\Delta})^2 \right) \tag{4}$$

and

$$T = \left(\frac{1}{2}(-1 - \sqrt{\Delta}), \frac{1}{4 s_2}(-1 - \sqrt{\Delta})^2 \right). \tag{5}$$

The system DM2D is bistable with two well-defined basins of attraction in the interval $0 \leqslant \Delta < 1$. The saddle point E is the edge state of the system, whereas L and T are attractors. The basins of attraction of L and T are separated by a smooth edge manifold $\mathcal{W}^s(E)$ of the strong type according to the typology in Ref. [14]. A phase portrait for $s_1 = -0.1875$ and $s_2 = -1$ is shown in Fig. 2. The parameters s_i, $i = 1, 2$, can

be re-interpreted as $s_i = -k_i^2 / R$, where $-k_i^2$, $i = 1, 2$, arise from a Laplacian in Fourier space, and R is a parameter akin to the Reynolds number in hydrodynamics. This phase portrait is ubiquitous in many fields of physics and turns out to be particularly convenient since only fixed points are present, while no chaotic dynamics takes place.

B. The autonomous 3D model

We extend the DM2D by introducing a third variable x_3 in the model, orthogonal to x_1 and x_2. The extension is such that (i) the laminar state L will be unstable along this new direction, (ii) the model still obeys the constraints on L and $N(x)$, and (iii) the dynamics within the 2D plane $\mathcal{P}$ defined by $x_3 = 0$ stays unchanged, i.e., $\mathcal{P}$ is an invariant plane for the new dynamics. The extended model reads

$$\frac{dx_1}{dt} = s_1 x_1 + x_2 + x_1 x_2, \tag{6}$$

$$\frac{dx_2}{dt} = s_2 x_2 - x_1^2 + \sigma x_3^2, \tag{7}$$

$$\frac{dx_3}{dt} = s_3 x_3 - \sigma x_2 x_3, \tag{8}$$

where s_3 and σ are two additional parameters of the model. The three-dimensional system is symmetric with respect to $\mathcal{P}$, which is an invariant plane and cannot be crossed by trajectories, so that we need only focus on the dynamics in the half-space $x_3 \geqslant 0$. The case for which the model is investigated is $s_1 = -0.1875$, $s_2 = -1$, and $\sigma = -1$. The control parameter for this study is s_3. By construction, the dynamics restrained to $\mathcal{P}$ is unaltered compared to the 2D model even as s_3 varies, and is completely determined by the state portrait of Fig. 2. However, the stability of L, E, and T in the direction x_3 transverse to $\mathcal{P}$ is now dependent on the value of s_3.

C. Parametric study

We explore the dynamics of the DM3D model by performing a parametric study in s_3 with a focus on the topological changes of the state space and the properties of the edge manifold for the half-space $x_3 \geqslant 0$. The amplitude $A = \|x\|$ (with $\| \cdot \|$ the Euclidian norm) of all fixed points and limit cycles is shown in a bifurcation diagram with respect to s_3 in Fig. 3(a). The real parts of the eigenvalues λ_r associated with each fixed point of the system are shown in Fig. 3(b) with the convention that a positive real part indicates instability. They are used to assess the type of bifurcation undergone by the steady states of Fig. 3(a).

The bifurcation diagram starts at $s_3 < 0$, for which the model has the same three fixed points—L, T, and E—as the original DM2D model. The only fixed point with an eigenvalue with a positive real part is the saddle point E. The associated three-dimensional state space is shown in Fig. 4(a) for $s_3 = -0.1$. Here, the two stable fixed points L and T each possess their basin of attraction, respectively $\mathcal{B}(L)$ and $\mathcal{B}(T)$. The intersection of their closures, the edge manifold, coincides exactly with $\mathcal{W}^s(E)$, thus

$$\mathcal{W}^s(E) = \overline{\mathcal{B}(L)} \cap \overline{\mathcal{B}(T)}. \tag{9}$$
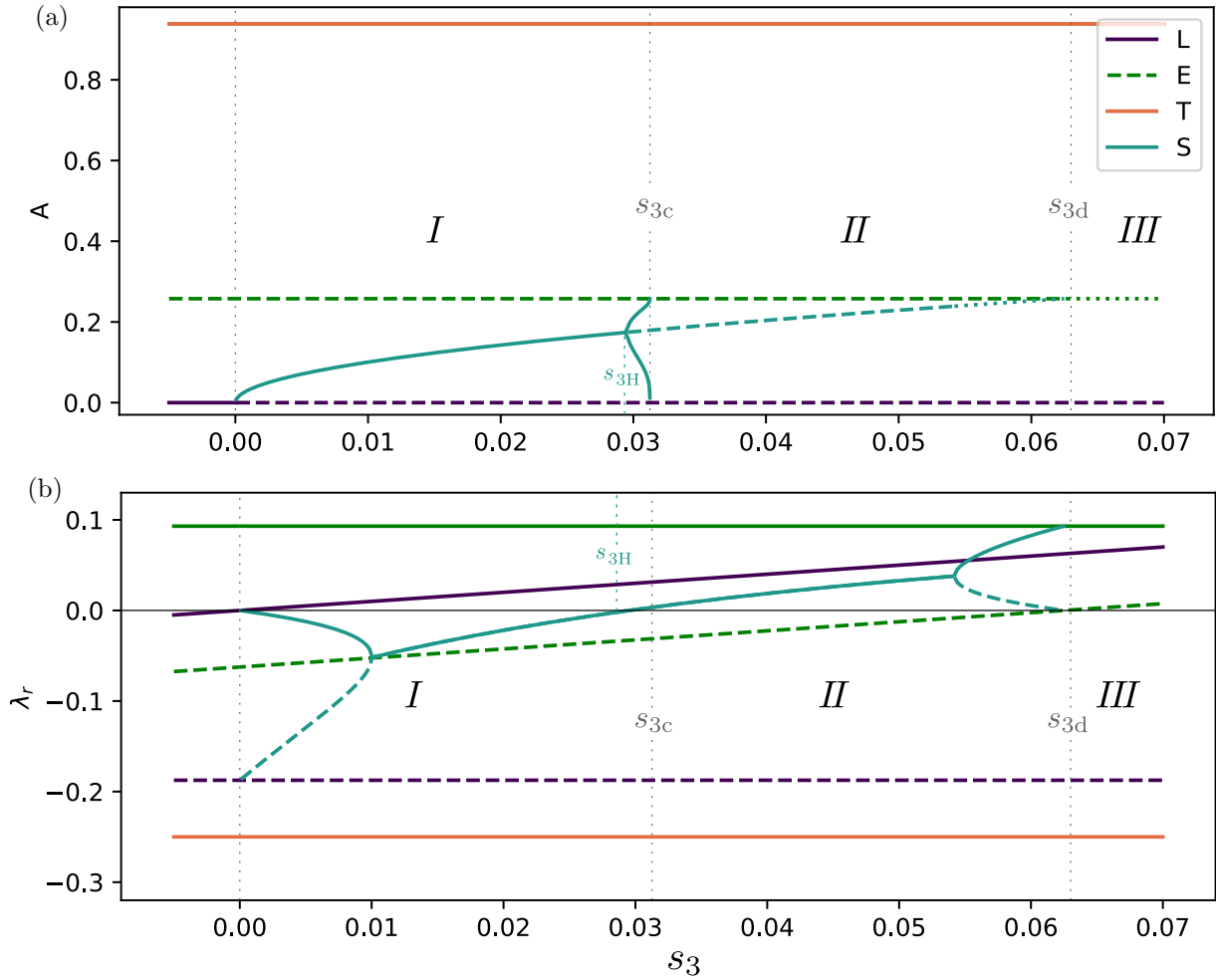
FIG. 3. (a) Bifurcation diagram for the autonomous DM3D model. Amplitude A of the steady and periodic solutions (minimum and maximum value only) vs s_3. Stable solutions (solid lines), and solutions with one (dashed lines) or two unstable eigenvalues (dotted lines). The limit cycle $\mathcal{C}$ appears at $s_3 = s_{3H} \approx 0.03$ and collapses at $s_3 = s_{3c} \approx 0.032$. (b) Real part of the eigenvalues of the linearized operator around each fixed point of the system vs s_3. The eigenvalues corresponding to perturbations of L, E, and T within the plane $\mathcal{P}$ do not evolve with s_3. The fixed point S arises as L, loses its linear stability at $s_3 = 0$, and disappears by merging with E at $s_3 = s_{3d} \approx 0.063$. Largest (solid) and second largest eigenvalue (dashed). Eigenvalues with real part $\leqslant -0.35$ are not shown. Vertical gray lines delimit the regions I, II, and III. The regions and parameters s_{3H}, s_{3c}, and s_{3d} are described in the text.

$\mathcal{W}^s(E)$ is for $s_3 < 0$ a two-dimensional surface invariant along x_3. It separates the basins of attraction of L and T and is then a codimension-1 manifold of the strong type.

For $s_3 > 0$ the laminar fixed point L becomes linearly unstable, as the real part of its largest eigenvalue crosses 0. For small enough $s_3 > 0$ the trajectories starting within the neighborhood of L are attracted toward a new fixed point S. This new fixed point emerges by construction in a supercritical pitchfork bifurcation at $s_3 = 0$ (we focus only on the branch with $x_3 > 0$). The stability of E and T in the new state space remains unchanged, as shown in Fig. 3(b). $\mathcal{W}^s(E)$ is no longer invariant along x_3 and starts to curl around S, illustrated in Fig. 4(b). However, the two basins of attraction of T and S (no longer L) exist and are separated by the edge manifold, which still coincides with $\mathcal{W}^s(E)$.

For $s_3 \gtrsim 0.01$, S is still stable but its leading eigenvalues are oscillatory: trajectories leaving L now spiral in toward S.

For $s_3 = s_{3H} \approx 0.0296$, S becomes unstable in a supercritical Hopf bifurcation, through which a stable limit cycle $\mathcal{C}$ is created. This limit cycle grows in amplitude until $s_3 = s_{3c} \approx 0.03125$, where a global bifurcation takes place. The state space just before and after s_{3c} is displayed in Fig. 5, and the global bifurcation is analyzed in more detail in Sec. II D. The state space continues to evolve beyond this global bifurcation. For $s_3 = 0.055$ the couple of complex conjugate eigenvalues of S become two distinct real positive eigenvalues. For $s_3 = s_{3d} = 0.063$ the additional fixed point S, which was created at $s_3 = 0$, merges with the saddle point E in a pitchfork bifurcation. Beyond $s_3 = 0.063$ the saddle point E still exists but has now two unstable eigenvalues as revealed by Fig. 3(b). The new unstable direction implies that all trajectories starting outside $\mathcal{P}$ converge toward T. This makes T the only attractor of the system. The investigation has been pushed to $s_3 = 0.07$ without an obvious change of state space topology.
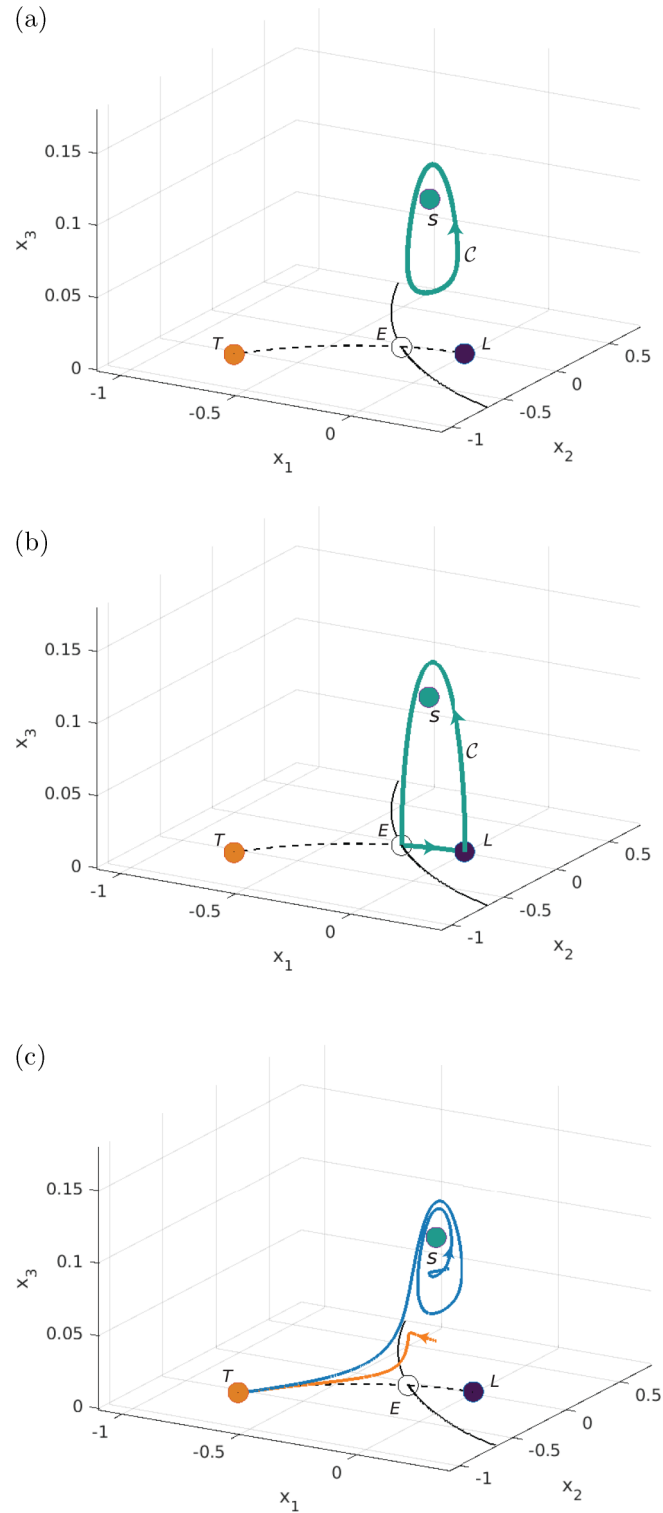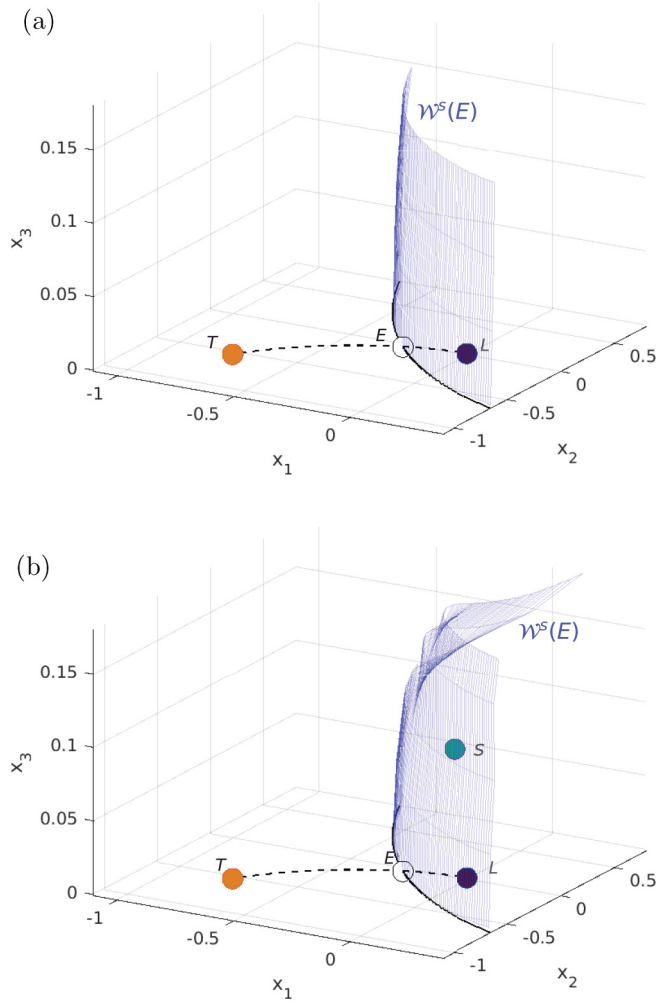
(a)

(b)

FIG. 4. Autonomous DM3D. Comparison between region $s_3 < 0$ and I. Phase portraits for different values of s_3: (a) $s_3 = -0.1$, (b) $s_3 = 0.01$. Surfaces (blue) correspond to the edge manifold $\mathcal{W}^s(E)$ identified using the method described in Ref. [11], Sec. II B.

D. Global bifurcation of the state space

This subsection is devoted to a more detailed analysis of the global bifurcation taking place at $s_{3c} \approx 0.031\,25$, because of its importance for the state space topology. Before the bifurcation, the limit cycle $\mathcal{C}$ grows in amplitude, as shown in Fig. 6(a), and the minimum distances between $\mathcal{C}$ and both E and L decrease as s_3 approaches s_{3c}. The two distances both scale algebraically with $\|s_3 - s_{3c}\|$, and, importantly, these two distances reach zero at the same value of $s_3 = s_{3c}$ (determined to numerical accuracy using double precision arithmetic). The period of the limit cycle $\mathcal{C}$ is also monitored as a function of $\|s_3 - s_{3c}\|$ in Fig. 6(b): a logarithmic fit of the form $T_p \sim \ln(|s_3 - s_{3c}|)$ is valid over as much as eight decades. This is an unambiguous signature for a saddle-loop collision [35,41]. Note that compared to [41], where the collision takes place between an attracting limit cycle and a saddle point, in the present case $\mathcal{C}$ collides simultaneously with two saddle points (however, the scaling for the diverging period T_p does not change).

(a)

(b)

(c)

FIG. 5. Autonomous DM3D. Comparison between regions I and II. Phase portraits for different values of s_3 close to the global bifurcation: (a) $s_3 = 0.031$. The system presents a hard edge between $\mathcal{C}$ and T, region I, (b) $s_3 = 0.031\,25$. Heteroclinic cycle close to s_{3c}, (c) $s_3 = 0.032$, beyond s_{3c} the heteroclinic connection collapses and the edge $\mathcal{W}^s(E)$ becomes of the weak kind, region II. The blue and orange trajectories illustrate the two newly born different routes to transition.
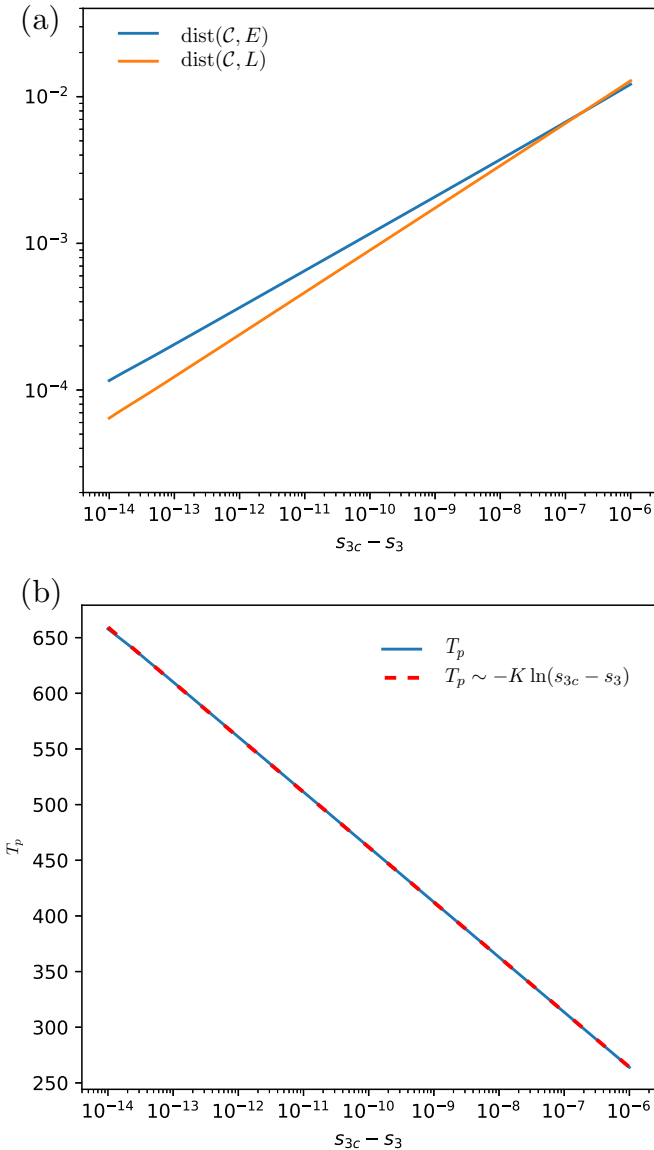
FIG. 6. (a) Minimum distance from the E/L-state to $\mathcal{C}$ as a function of the distance to criticality. (b) Period T_p of the limit cycle $\mathcal{C}$ vs the distance to criticality (solid), logarithmic fit with slope $K = 49.4$ (dashed). The critical $s_{3c} \approx 0.031\,25$.

At the bifurcation point, E and L form a heteroclinic network: the heteroclinic connection from E to L lies in the invariant plane $\mathcal{P}$ whereas the connection from L to E lies outside $\mathcal{P}$. The bifurcation occurs as $\mathcal{C}$ collides with the heteroclinic cycle connecting E to L. Close to criticality, $\mathcal{C}$ deforms close to the fixed points, as seen in Fig. 5(b).

Just before the global bifurcation takes place, there are still two basins of attraction, respectively $\mathcal{B}(T)$ and $\mathcal{B}(\mathcal{C})$. The intersection of their closures, the edge manifold, coincides with $\mathcal{W}^s(E)$. However, once the heteroclinic connection is formed, the manifold separating the two different basins of attraction becomes of the weak type, as illustrated by its state space in Fig. 5(c), where trajectories following the two newly born routes to transition are shown. The global bifurcation changes the whole structure of the state space in the following way: for $s_3 > s_{3c}$, the two disjoint different basins of attraction

no longer exist as open sets. All trajectories starting outside $\mathcal{P}$ asymptotically approach T in forward time. Note that trajectories starting strictly in $\mathcal{P}$ can still reach L provided they belong to the relevant part [which coincides with the embedding in $\mathbb{R}^3$ of the basin $\mathcal{B}(L)$ from DM2D]; however, $\mathcal{P}$ is no longer an open set in $\mathbb{R}^3$ and has measure zero.

A useful measure to understand the state space is the transition time τ_{tr}, introduced in [26] as the time it takes for a trajectory to approach the turbulent attractor within a given predetermined (small) distance ϵ_T, as a function of the starting point $\boldsymbol{x}$. Mathematically it is defined as $\arg\min_{t>0}\|\phi^t(\boldsymbol{x}) - T\| < \epsilon_T$, where ϕ^t refers to the flow map. Iso-$x_2 = -0.2$ cross-sections of the transition time for $s_3 \lesssim s_{3c}$ and $s_3 \gtrsim s_{3c}$ shown in Figs. 8(a) and 8(b), respectively, confirm that only the basin of attraction $\mathcal{B}(T)$ is left. The stable manifold of E, $\mathcal{W}^s(E)$, still exists as a codimension-1 manifold except that it appears now wound around S. It is now possible to distinguish a faster and a slower route to turbulence, depending on which side of $\mathcal{W}^s(E)$ the initial condition is located. As a consequence, the edge manifold is no longer interpretable as a basin boundary, but rather as a soft boundary in state space between two routes to transition.

E. E as an edge state

The interpretation of the edge manifold, beyond criticality, as a manifold separating two different routes, one fast and one slow, to the same attractor holds for the parametric region of interest after the global bifurcation. There exists, however, a fundamental difference between two behaviors, for $s_3 \in (0.03125, 0.063)$ and $s_3 > s_{3d} = 0.063$, linked to the notion of *accessibility* similar to that used in Ref. [42] and the number of unstable directions of E, which define whether it is an edge state or not.

For low $s_3 < s_{3d}$, E has only one unstable eigenvalue, and its unstable manifold is fully contained in $\mathcal{P}$. This behavior is illustrated in the state portrait in Fig. 9(a). It is hence possible to approach E using a trajectory starting outside $\mathcal{P}$, and E is labeled as *accessible*. This is shown in the time series of three trajectories with nearby initial conditions in Fig. 9(c), where the edge trajectory approaches E starting from an initial condition with $x_3(0) \neq 0$ and remains in its neighborhood (at least transiently). However, for $s_3 > 0.063$, E has two distinct unstable eigenvalues, and is now also repelling in the direction transverse to $\mathcal{P}$. Finding a trajectory converging toward E from an initial condition outside $\mathcal{P}$ is now impossible. E is said to be *nonaccessible*. This behavior is illustrated using a phase portrait in Fig. 9(b) and using the time series corresponding to three trajectories starting from nearby initial conditions in Fig. 9(d): unlike in Fig. 9(a), we observe now that the trajectory sandwiched between the fast and slow routes in state space does not approach E. Consequently, the trajectories close to the edge manifold that follow the slow route do not visit the neighborhood of E.

The notion of accessibility of a given fixed point is directly related here to the codimension of its stable manifold. Here the saddle point E is accessible when $\mathrm{codim}\,(\mathcal{W}^s(E)) = 1$, in which case E is an edge state, and it is nonaccessible when $\mathrm{codim}\,(\mathcal{W}^s(E)) > 1$, in which case the system does not have any edge state. Note how this is dependent on dimensions:
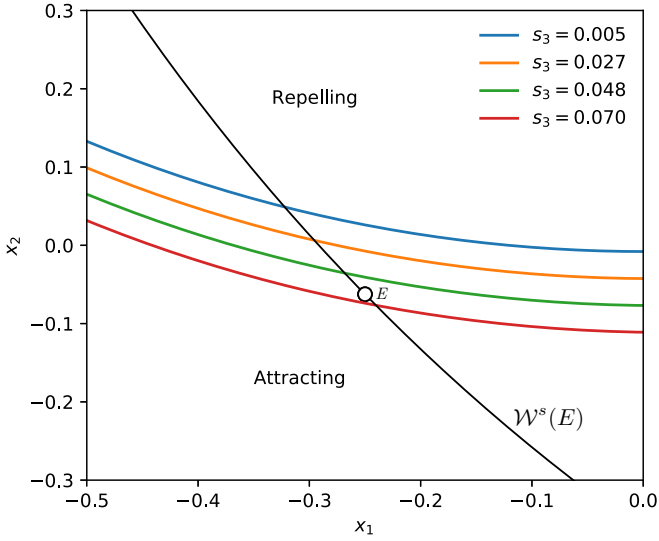
FIG. 7. Transverse FTLE at $x_3 = 0$ for a time horizon $\tau = 1$. The solid black line indicates $\mathcal{W}^s(E)$. Color lines indicate the 0-isovalue of the transverse FTLE for different s_3.

for any s_3 the system DM2D restrained to $\mathcal{P}$, which is of dimension 2 only, possesses E as an edge state. A simple local diagnostic for the instability of E in a direction transverse to the invariant plane $\mathcal{P}$ consists in computing the transverse finite-time Lyapunov exponent (FTLE) λ_T. For any $\boldsymbol{x} \in \mathcal{P}$, we define P_3 as the projection on $\mathcal{P}^\perp$ such that $P_3(x_1, x_2, x_3) = (0, 0, x_3)$, and

$$\lambda_T(\boldsymbol{x}, \tau) = \frac{1}{\tau} \log \left(\frac{\|P_3(\phi^\tau(\boldsymbol{x}))\|}{\|P_3(\boldsymbol{x})\|} \right). \tag{10}$$

A point $\boldsymbol{x} \in \mathcal{P}$ such that $\lambda_T(\boldsymbol{x}, \tau) > 0$ for τ sufficiently small is nonaccessible from outside $\mathcal{P}$. Isolevels of transverse FTLEs are shown in Fig. 7 for the horizon time $\tau = 1$. By construction λ_T is always positive at $\boldsymbol{x} = L$ as soon as $s_3 > 0$, whereas at $\boldsymbol{x} = T$ it is negative since T is always stable. The locus where λ_T crosses zero hence marks the stability boundary in $\mathcal{P}$ between trajectories initially deviating from $\mathcal{P}$ and those attracted by $\mathcal{P}$. The isoline $\lambda_T = 0$ (for a given value of τ) moves with changing s_3. From Fig. 7 it is clear that E lies on the negative side of the stability boundary for $s_3 < s_{3d}$ and on the positive side for $s_3 > s_{3d}$. $s_3 = s_{3d}$ hence marks the loss of accessibility of E. This has strong implications for the bisection process and the numerical determination of the edge state. When E is accessible, a one-dimensional search (i.e., a bisection) along almost any line in state space will generate one trajectory converging to E (even if this trajectory is repelling). When E is not accessible, this is no longer the case and the bisection algorithm is not expected to converge from any initial condition: there is no edge state, although E still exists as a saddle point. Concretely, E cannot be defined as an edge state but it is still an exact solution of the system. To find E, the only possibility is to apply a control strategy that leaves E unchanged but affects its effective transverse stability. Any control strategy that can make $\lambda_T(E, \tau)$ negative for some value of τ is likely to make bisection algorithms converge to E. This differentiation of accessible or nonaccessible is particularly relevant to understand the failure of the
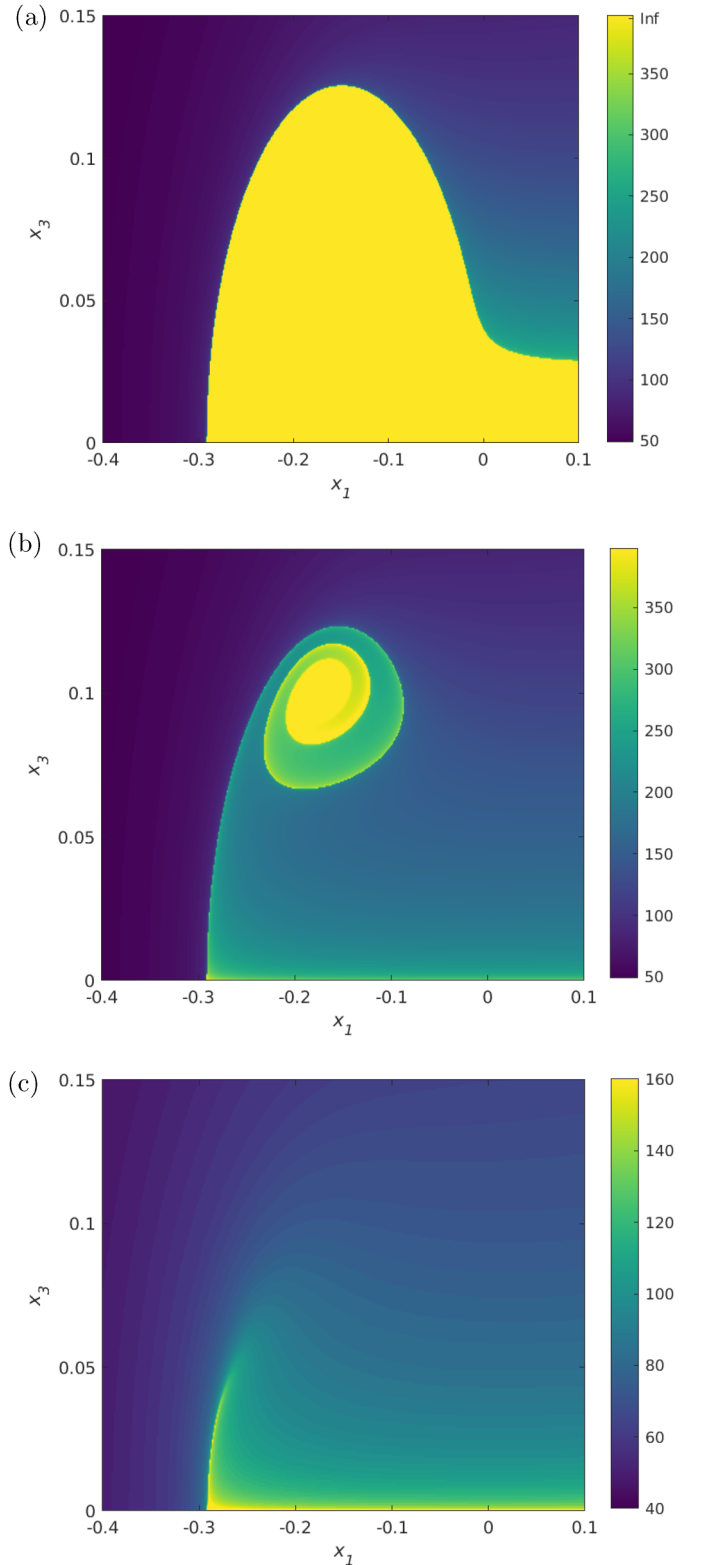

FIG. 8. Transition times τ_{tr} for the $x_1 x_3$-plane for $x_2 = 0$: (a) $s_3 = 0.031\,249$ within region I, (b) $s_3 = 0.032$ within region II, and (c) $s_3 = 0.065$ within region III.

bisection algorithm and to determine E's role as a mediator of subcritical transition.

The loss of accessibility of the edge state is further illustrated in Fig. 8(c) using transition times computed in a section
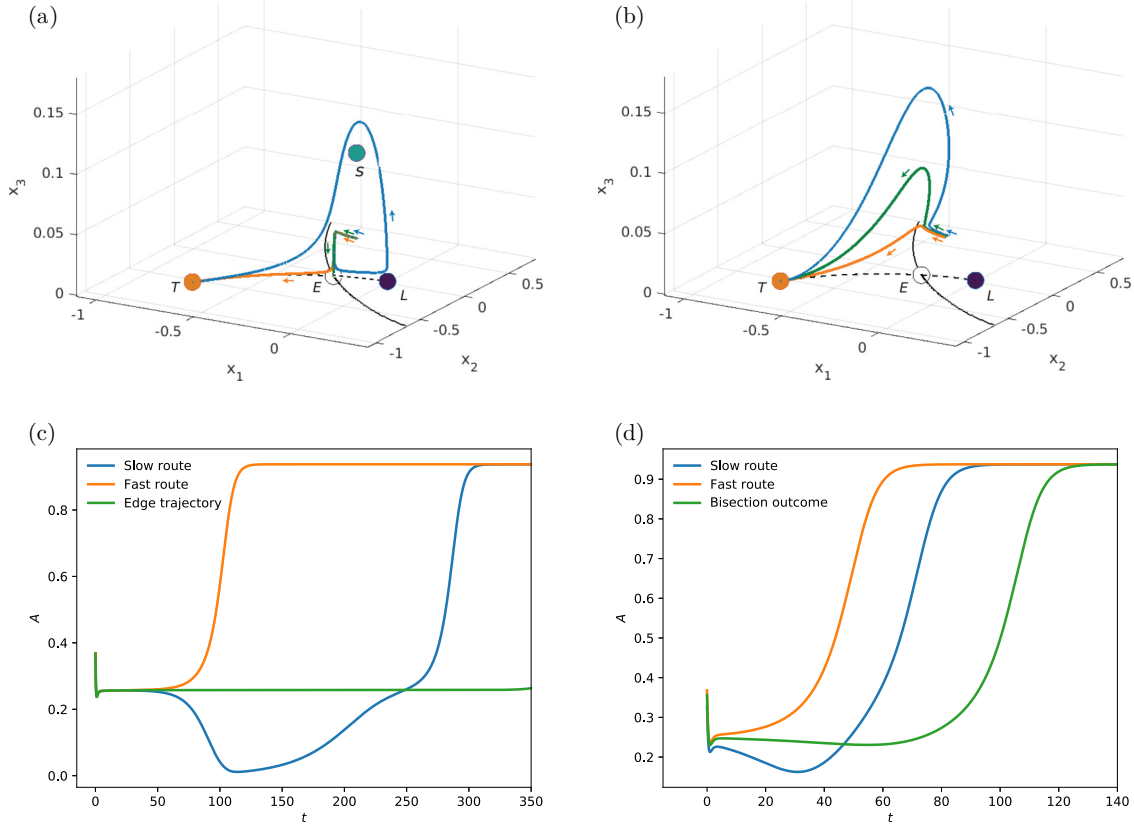
FIG. 9. Comparison between region II and III. Trajectories on different sides of the edge manifold starting from initial conditions with $x_3 = 0.05$. (a) $s_3 = 0.032$, the edge state is accessible by bisection from outside $\mathcal{P}$, region II. (b) $s_3 = 0.065$, the edge state is no longer accessible by bisection from outside $\mathcal{P}$, region III. (c) Time series for $A(t)$ for the trajectories in (a). (d) Idem for the trajectories in (b). The blue and orange trajectories illustrate the two newly born different routes to transition, to be compared with the same colors in Fig. 1(b).

with $x_2 = -0.05$. The figure highlights larger values of τ_{tr} in some regions of the state space; however, the highlighted structure outside $\mathcal{P}$ diffuses out and is not a sharp boundary for the trajectories on either sides, in contrast to Figs. 8(a) and 8(b).

III. THE NONAUTONOMOUS 3D MODEL

The autonomous model DM3D has the discriminant Δ, or indirectly the Reynolds number R, as a control parameter, as is the case for, e.g., plane Poiseuille flow. In an effort to mimic the evolution of a localized disturbance in a spatially developing flow, one needs to take into account the fact that the disturbance experiences changing values of R as it is advected downstream at an approximately constant velocity. The simplest way to introduce a time dependence in the DM3D model is to make the growth rate s_3 time-dependent, so that it becomes positive only at a finite time and continues to increase subsequently. This ensures that L, E, and T are still fixed points of the system for every time. A linear relation of the type $s_3(t) = k_1 t + k_2$ fulfills these requirements with as few parameters as possible. The system then becomes nonautonomous, while retaining all the properties required for models of subcritical transition. It reads

$$\frac{dx_1}{dt} = s_1 x_1 + x_2 + x_1 x_2, \tag{11}$$

$$\frac{dx_2}{dt} = s_2 x_2 - x_1^2 + \sigma x_3^2, \tag{12}$$

$$\frac{dx_3}{dt} = (k_1 t + k_2) x_3 - \sigma x_2 x_3. \tag{13}$$

The time interval is restrained to $t \in [t_0, t_0 + T_F]$, with $k_1 = 0.73/T_F$ and $k_2 = -0.1$, in order to facilitate the comparison with its autonomous counterpart.

A state portrait of the nonautonomous system is shown for several trajectories with $t_0 = 0$ and $T_F = 350$ in Fig. 10(a). The chosen trajectories start very close to the edge manifold within $\mathcal{P}$ from an initial condition with $x_3(t_0) = 10^{-6}$, with color coding chosen to match Fig. 1 and Figs. 9(a) and 9(b). The time series for the amplitude along the trajectories are plotted in Fig. 10(b). The fixed point T in DM3D can be reached in two different ways from outside the $x_1 x_2$ plane, either approaching L (slow route) or not (fast route), as shown in Fig. 10(a). The model experiences thus a Blasius-like dynamics when considering trajectories starting at a weak nonzero distance from the invariant plane $\mathcal{P}$, as suggested by comparing Figs. 10(a) and 1(b).
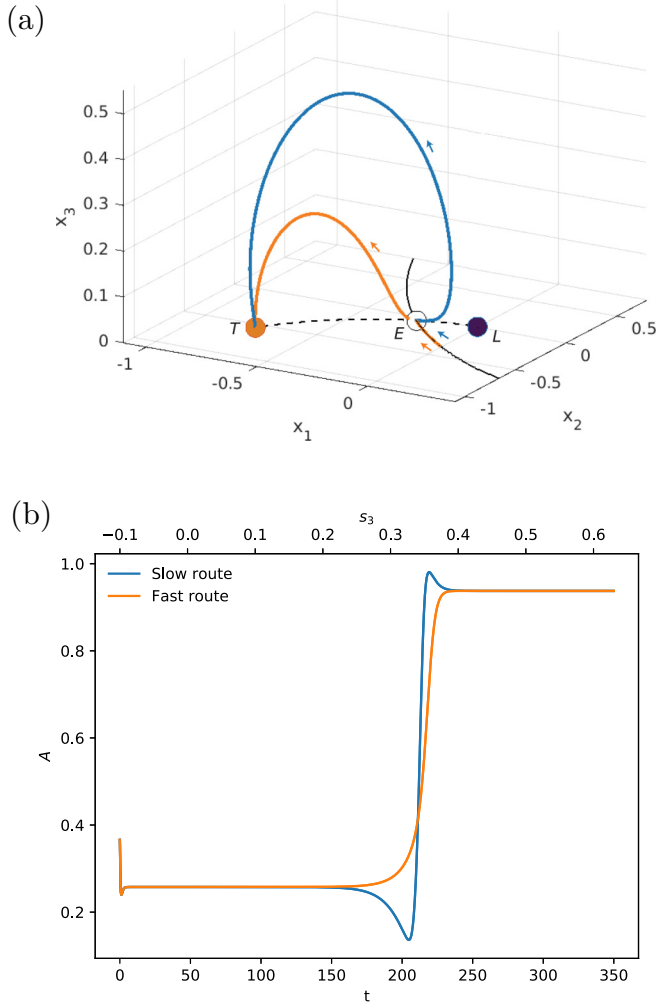
(a)

(b)

FIG. 10. DM3D nonautonomous model. (a) State portrait for two trajectories starting close to the edge of DM2D and to the invariant plane $\mathcal{P}$, (b) time series of the amplitudes $A(t)$ along the same trajectories.

IV. DISCUSSION

In the present article, we have devised and investigated two low-order models, one autonomous and the other nonautonomous. These models aim to explain nonstandard behaviors observed during bisection in bistable systems once one of the attractors undergoes a bifurcation and becomes unstable [15,25,26]. The present generalization respects the constraints due to the non-normality of the linearized operator as well as the energy-conserving nonlinearity due to the Reynolds-Orr theorem [19]. The procedure is not limited to the two-dimensional Dauchot-Manneville model, and it can be carried out in higher dimension using reference models such as, e.g., the four-dimensional Waleffe model [30]; however, the present three-dimensional model is ideal for visualizing state space boundaries.

The nonautonomous DM3D model has dynamics similar to DM2D as long as the new parameter $s_3 < 0$. As s_3 increases above zero, the laminar state L becomes unstable in favor of a new fixed point S. After a series of local bifurcations, S becomes a limit cycle $\mathcal{C}$. The first topological change occurs

at $s_3 = s_{3}c$ as $\mathcal{C}$ collides with the two saddle points E and L: the stable manifold $W^s(E)$ still exists as a codimension-1 manifold, but it does not split the state space into two any longer; instead, all trajectories outside the invariant plane $\mathcal{P}$ are attracted by the turbulent fixed point T. Past a second bifurcation at $s_3 = s_{3d}$, E gains one more unstable eigenvalue so that codim $(\mathcal{W}^s(E))$ goes from 1 to 2. $\mathcal{W}^s(E)$ is no longer the edge manifold and E is no longer the edge state because it has lost its accessibility property, and the edge has collapsed, i.e., there is no edge anymore. The only possibility to reach E from outside $W^s(E)$ $\mathcal{P}$ is to use a control strategy in order to restabilize the laminar state L locally.

The present extension of a low-order model for a subcritical transition allows for a more generic investigation of bistable systems, when a linear instability disturbs the usual dynamical picture. It also paves the way for the study of the edge manifold beyond criticality in higher-dimensional systems, such as the full Navier-Stokes equations. In fluid systems there are several canonical examples where both transition scenarios are present, such as plane Poiseuille flow [26], the Blasius boundary layer [15], or bent pipe flow [25]. Although a detailed comparison of these flow cases with the present models would be naive, common features related to the global topology of the state space are relevant. The bent pipe flow system investigated in Ref. [25] is the simplest case: it contains two attractors, like in any bistable system, except that a nontrivial state (a traveling wave) has inherited the former stability of the laminar flow via a local supercritical bifurcation. Although the precise nature of the bifurcation differs, this situation is topologically similar to the autonomous model DM3D for $0 < s_3 < s_{3c}$: two basins of attraction separated by a strong edge manifold, including a limit cycle on one side. The plane Poiseuille flow configuration investigated in Ref. [26] for R = 5855 is more complex: the edge state solution still exists, whereas there is only one attraction basin, namely the turbulent basin. This is analogous to the state space picture of the autonomous model for $s_{3c} < s_3 < s_{3d}$, where the edge manifold still exists as a codimension-1 hypersurface except that it does not split the state space into two disjoint regions any longer. Eventually, the case of the Blasius boundary layer, shown in Fig. 1, is the most complex: although early time bisection seems to indicate that the edge state is accessible along a trajectory starting from a well-tuned initial condition, it is lost for larger times. The early and later times can be informally compared to the lower and higher $s_3 > 0$ regimes of the DM3D model, respectively below and above s_{3d}. The nonautonomous model, by construction, sweeps as time progresses through the same range of values of s_3 as its autonomous counterpart. As shown in Fig. 10, initial conditions that are close to, yet outside, the invariant plane $\mathcal{P}$ would first shadow the edge trajectory in $\mathcal{P}$. At a later time they would be ejected away from $\mathcal{P}$ and converge toward the turbulent set T in two possible ways: either via a transient approach to L (blue trajectories in Fig. 10) or without it (orange trajectories in Fig. 10). The edge manifold is only defined for short finite times but does not exist as an invariant set over unbounded times. The edge state is not accessible anymore except from initial conditions strictly inside $\mathcal{P}$, or at the cost of a control strategy. This confirms and explains

the conclusions of Ref. [15] based on costly edge tracking of the Navier-Stokes equations in large computational domains (cf. both their Fig. 10 and the present Fig. 1 compared to the current Fig. 10).

The two models presented here are simple, nonchaotic, and their three-dimensional state space has the important advantage of being easily visualizable. Yet they offer the possibility to understand the topology of seemingly hopelessly tangled high-dimensional state spaces associated with several fluid problems. We believe that the present strategy can be used in many diverse areas of physics where deterministic bistability is disturbed by an additional local bifurcation.

[1] O. Reynolds, An experimental investigation of the circumstances which determine whether the motion of water shall be direct or sinuous, and of the law of resistance in parallel channels, P. R. Soc. London **35**, 84 (1883).

[2] B. Eckhardt, T. M. Schneider, B. Hof, and J. Westerweel, Turbulence transition in pipe flow, Annu. Rev. Fluid Mech. **39**, 447 (2007).

[3] H. E. Nusse and J. A. Yorke, Basins of attraction, Science **271**, 1376 (1996).

[4] P. G. Drazin and W. H. Reid, *Hydrodynamic Stability*, 2nd ed., Cambridge Mathematical Library (Cambridge University Press, Cambridge, 2004).

[5] T. Itano and S. Toh, The dynamics of bursting process in wall turbulence, J. Phys. Soc. Jpn. **70**, 703 (2001).

[6] J. D. Skufca, J. A. Yorke, and B. Eckhardt, Edge of Chaos in a Parallel Shear Flow, Phys. Rev. Lett. **96**, 174101 (2006).

[7] Y. Duguet, A. P. Willis, and R. R. Kerswell, Transition in pipe flow: The saddle structure on the boundary of turbulence, J. Fluid Mech. **613**, 255 (2008).

[8] T. M. Schneider and B. Eckhardt, Edge states intermediate between laminar and turbulent dynamics in pipe flow, Philos. T. R. Soc. A **367**, 577 (2008).

[9] A. P. Willis, Y. Duguet, O. Omel'chenko, and M. Wolfrum, Surfing the edge: Using feedback control to find nonlinear solutions, J. Fluid Mech. **831**, 579 (2017).

[10] M. Linkmann, F. Knierim, S. Zammert, and B. Eckhardt, Linear feedback control of invariant solutions in channel flow, J. Fluid Mech. **900**, A10 (2020).

[11] M. Beneitez, Y. Duguet, P. Schlatter, and D. S. Henningson, Edge manifold as a Lagrangian coherent structure in a high-dimensional state space, Phys. Rev. Research **2**, 033258 (2020).

[12] D. Sweet, H. E. Nusse, and J. A. Yorke, Stagger-and-Step Method: Detecting and Computing Chaotic Saddles in Higher Dimensions, Phys. Rev. Lett. **86**, 2261 (2001).

[13] B. Hof, J. Westerweel, T. M. Schneider, and B. Eckhardt, Finite lifetime of turbulence in shear flows, Nature (London) **443**, 59 (2006).

[14] N. R. Lebovitz, Boundary collapse in models of shear-flow transition, Commun. Nonlin. Sci. **17**, 2095 (2012).

[15] M. Beneitez, Y. Duguet, P. Schlatter, and D. S. Henningson, Edge tracking in spatially developing boundary layer flows, J. Fluid Mech. **881**, 164 (2019).

[16] Y. Duguet, P. Schlatter, D. S. Henningson, and B. Eckhardt, Self-Sustained Localized Structures in a Boundary-Layer Flow, Phys. Rev. Lett. **108**, 044501 (2012).

[17] J. Kühnen, P. Braunshier, M. Schwegel, H. Kuhlmann, and B. Hof, Subcritical versus supercritical transition to turbulence in curved pipes, J. Fluid Mech. **770**, R3 (2015).

[18] S. A. Orszag, Accurate solution of the Orr-Sommerfeld stability equation, J. Fluid Mech. **50**, 689 (1971).

[19] P. J. Schmid and D. S. Henningson, *Stability and Transition in Shear Flows* (Springer, 2001).

[20] M. V. Morkovin, On the many faces of transition, in *Viscous Drag Reduction* (Springer, 1969), pp. 1–31.

[21] M. A. Bucci, D. Puckert, C. Andriano, J.-C. Loiseau, S. Cherubini, J.-C. Robinet, and U. Rist, Roughness-induced transition by quasi-resonance of a varicose global mode, J. Fluid Mech. **836**, 167 (2018).

[22] A. Bottaro, P. Corbett, and P. Luchini, The effect of base flow variation on flow stability, J. Fluid Mech. **476**, 293 (2003).

[23] R. M. Clever and F. H. Busse, Three-dimensional convection in a horizontal fluid layer subjected to a constant shear, J. Fluid Mech. **234**, 511 (1992).

[24] T. Khapko, T. Kreilos, P. Schlatter, Y. Duguet, B. Eckhardt, and D. S. Henningson, Edge states as mediators of bypass transition in boundary-layer flows, J. Fluid Mech. **801**, R2 (2016).

[25] J. Canton, E. Rinaldi, R. Örlü, and P. Schlatter, Critical Point for Bifurcation Cascades and Featureless Turbulence, Phys. Rev. Lett. **124**, 014501 (2020).

[26] S. Zammert and B. Eckhardt, Transition to turbulence when the Tollmien-Schlichting and bypass routes coexist, J. Fluid Mech. **880**, R2 (2019).

[27] S. Cherubini, P. D. Palma, J.-C. Robinet, and A. Bottaro, Edge states in a boundary layer, Phys. Fluids **23**, 051705 (2011).

[28] In physical space, the coordinates x, y, z correspond to the streamwise, wall-normal, and spanwise directions. λ_2 is the criterion for vortex identification introduced in [43].

[29] O. Dauchot and P. Manneville, Local versus global concepts in hydrodynamic stability theory, J. Phys. II **7**, 371 (1997).

[30] F. Waleffe, On a self-sustaining process in shear flows, Phys. Fluids **9**, 883 (1997).

[31] C. Cossu, Non-linear optimal perturbations in subcritical instabilities, in *IUTAM Symposium on Laminar-Turbulent Transition and Finite Amplitude Solutions*. Fluid Mechanics and its Applications, edited by T. Mullin and R. Kerswell (Springer, Dordrecht, 2005), Vol. 77, pp. 251–266.

[32] J. Vollmer, T. M. Schneider, and B. Eckhardt, Basin boundary, edge of chaos and edge state in a two-dimensional model, New J. Phys. **11**, 013040 (2009).

[33] N. Lebovitz and G. Mariotti, Edges in models of shear flow, J. Fluid Mech. **721**, 386 (2013).

[34] M. Pausch and B. Eckhardt, Direct and noisy transitions in a model shear flow, Theor. Appl. Mech. Lett. **5**, 111 (2015).

[35] S. Strogatz, *Nonlinear Dynamics and Chaos: With Applications to Physics, Biology, Chemistry, and Engineering* (Westview Press, Boulder, CO, 2001).

[36] F. Marquardt, J. G. E. Harris, and S. M. Girvin, Dynamical Multistability Induced by Radiation Pressure in High-Finesse Micromechanical Optical Cavities, Phys. Rev. Lett. **96**, 103901 (2006).

[37] G. K. Nave Jr. and S. D. Ross, Global phase space structures in a model of passive descent, Commun. Nonlin. Sci. **77**, 54 (2019).

[38] L. N. Trefethen, A. E. Trefethen, S. C. Reddy, and T. A. Driscoll, Hydrodynamic stability without eigenvalues, Science **261**, 578 (1993).

[39] J. Bezanson, A. Edelman, S. Karpinski, and V. B. Shah, Julia: A fresh approach to numerical computing, SIAM Rev. **59**, 65 (2017).

[40] C. Rackauckas and Q. Nie, DifferentialEquations.jl A performant and feature-rich ecosystem for solving differential equations in Julia, J. Open Res. Softw. **5**, 15 (2017).

[41] P. Gaspard, Measurement of the instability rate of a far-from-equilibrium steady state at an infinite period bifurcation, J. Phys. Chem. **94**, 1 (1990).

[42] C. Grebogi, E. Ott, and J. A. Yorke, Basin boundary metamorphoses: changes in accessible boundary orbits, Nucl. Phys. B **2**, 281 (1987).

[43] J. Jeong and F. Hussain, On the identification of a vortex, J. Fluid Mech. **285**, 69 (1995).